Models of the Structure and Gating Mechanisms of the Pore Domain of the NaChBac Ion Channel

Yinon Shafrir, Stewart R. Durell, and H. Robert Guy

Laboratory of Cell Biology, CCR, National Cancer Institute, National Institutes of Health, Bethesda, Maryland 20892-5567

ABSTRACT The NaChBac prokaryotic sodium channel appears to be a descendent of an evolutionary link between voltage-gated K_V and Ca_V channels. Like K_V channels, four identical six-transmembrane subunits comprise the NaChBac channel, but its selectivity filter possesses a signature sequence of eukaryotic Ca_V channels. We developed structural models of the NaChBac channel in closed and open conformations, using K^+-channel crystal structures as initial templates. Our models were also consistent with numerous experimental results and modeling criteria. This study concerns the pore domain. The major differences between our models and K^+ crystal structures involve the latter portion of the selectivity filter and the bend region in S6 of the open conformation. These NaChBac models may serve as a stepping stone between K^+ channels of known structure and Na_V, Ca_V, and TRP channels of unknown structure.

INTRODUCTION

Understanding the structure and functional mechanisms of voltage-gated channels remains a major goal in membrane biophysics. Recently determined crystal structures (Protein Data Bank identifications 1orq, 2a79, 2r9r, and 3beh) (1–4) have advanced our understanding of K^+ channels dramatically. However, the structures of Na_v and Ca_v channels remain unknown. Evolutionary analyses strongly suggest that eukaryotic voltage-gated Na_v and Ca_v channels evolved from K_v channels (5). All of these proteins possess a six-transmembrane (6TM) motif in which a voltage-sensing domain (VSD), formed by S1–S4, precedes a pore domain (PD) formed by the S5-P-S6 segments, where P represents a re-entrant loop that forms the selectivity filter. Only one 6TM motif occurs in the primary α-transmembrane subunit of most K_v channels, whereas the α-subunit of most eukaryotic Ca_v and Na_v channels has four homologous 6TM motifs. The notable exceptions are CatSper channels that have only one 6TM motif per α-subunit (6), and some putative fungal Ca^{2+} channels that have two 6TM motifs per α-subunit (7). Sequences of numerous prokaryotic families of K^+ channels were observed. However, prokaryotic sequences that are more closely related to eukaryotic Ca_v and Na_v channels appear to be limited to a single family of relatively closely related sequences that, like K_v channels, have only one 6TM motif per subunit. This family includes NaChBac. We chose to model NaChBac channels because of their unique position with respect to the more well-known families of K_v, Na_v, and Ca_v. Like K_v, NaChBac is composed of four identical repeats. It possesses the same selectivity signature sequence as Ca_v channels, but is permeable to Na^+ cations, similar to Na_v channels. From a modeling point of view, NaChBac presents an exciting opportunity to form a link between the known structures of K_v channels and the distantly related sequences of the Ca_v and Na_v superfamilies.

We present structural models of the transmembrane region and connecting loops of the NaChBac channel from *Bacillus halodurans*. Ribbon representations of our NaChBac models of open or densensitized and closed conformations of the pore domain are illustrated in Fig. 1. Coordinates for our models are provided in the Supplementary Material. The rationale for these models, and their similarities and differences from K_v channels, are described in Results.

When we originally identified the first NaChBac sequence in the *Bacillus halodurans* genomic database (8), we proposed that it formed a Ca_v channel, based on the sequence similarity of its P segment to those of eukaryotic Ca_v channels. Specifically, its sequence contains an FxxxTxExW signature found in the P segment of all four 6TM domains of the vast majority of eukaryotic Ca_v channels, but which is altered in Na_v channels. However, expression of the protein in eukaryotic cells revealed that this sequence in fact codes for a Na^+-selective channel (6). Further studies by Yue et al. (9) revealed that substitution of either residue S192 or S195 by a negatively charged aspartate increases the Ca^{2+} conductivity twofold with respect to Na^+. A double substitution of both residues makes the channel highly selective for Ca^{2+} (9). These findings suggest that the selectivity filter of Ca_v channels is more electronegative than that of NaChBac. Most eukaryotic Ca_v channels have negatively charged residues in some 6TM motifs at positions analogous to S192 and S195, but never as many as in these mutants (because of the four-fold symmetry of NaChBac), and often some of these additional negatively charged residues are offset by additional positively charged residues at other positions within the P segments. Thus, other factors in addition to the net charge may be involved in determining selectivity.

Submitted April 15, 2008, and accepted for publication June 30, 2008.

Address reprint requests to H. Robert Guy, Laboratory of Cell Biology, CCR, National Cancer Institute, National Institutes of Health, 12 South Dr., Bethesda, MD 20892-5567. Tel.: 301-496-2068; Fax: 301-402-4724; E-mail: bg4y@nih.gov.

Editor: Francisco Bezanilla.

0006-3495/08/10/3650/13 $2.00

doi: 10.1529/biophysj.108.135327

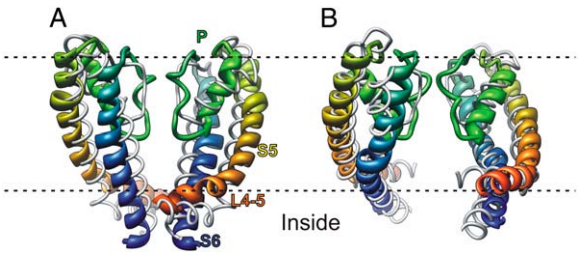

FIGURE 1 Ribbon representation of NaChBac model pore domains colored from orange to blue, superimposed on template structures represented by gray tubes. Each tetramer is composed of four identical subunits, only two of which are shown in these side views. Labels indicate L4–5, S5, P, and S6 segments. (*A*) Closed conformation model compared with MlotiK template. (*B*) $Open_2$ conformation model compared with Kv1.2 template.

Another puzzle introduced by this channel is its activation mechanism. The activation gate is formed by the S6 segment. The most highly conserved S6 residue among NaChBac homologues is N225. This conservation pattern is also true for Ca_v, Na_v, and even TRP channels. In contrast, aspargine is not conserved at the analogous position in any K_v family. As discussed below, this difference may result in a very different gating mechanism in NaChBac compared with the known mechanism of the K_v family. Zhao et al. (10) conducted a study that may hint at the nature of this difference, in which a single mutation from the leucine (L226) that immediately follows the conserved asparagine to a proline completely reversed the activation of NaChBac with respect to the membrane's polarization. As far as we know, no equivalent mutation can cause this reversal in K_v channels. Our models attempt to explain why N225 is so important to the gating mechanism. Our accompanying article proposes how gating of the PD is coupled to voltage-dependent movements in the VSD.

Like most voltage-gated channels, NaChBac inactivates at positive voltages (11). The transition between open and inactivated conformations is poorly understood, but may be much smaller and more subtle than transitions between resting and open conformations. We developed our open-conformation models so that the central pore would be large enough to allow the passage of Na^+ ions. Constraining the static models to fourfold symmetry around the major axis of the pore helped prevent the formation of permeation barriers by hydrophobic or positively charged groups. However, when these constraints were removed during molecular-dynamics (MD) simulations, we occasionally observed asymmetric collapses of the selectivity filter that occluded the pore, and one or two positively charged side chains sometimes entered the pore. Thus, it is difficult to know whether the ''open'' models actually correspond better to open, flickering, or inactivated conformations, especially because some of the data used in developing these models actually derive from inactivated rather than activated channels. Our studies emphasize the activation rather than inactivation mechanism. Thus, we chose to call these models ''open'', to avoid the misconception that we are attempting to model the inactivation mechanism.

METHODS

Initial models were developed with essentially the same procedure that we used successfully to model structures of K^+ channels in the absence of crystal structures, except that here we use known crystal structures of homologous proteins as an initial template. First, generic NaChBac α-helices were matched to helical segments of Kv1.2 (3), KvAP (1), and KcsA (Protein Data Bank identification 1k4c) crystal structures (12). These generic helices were developed with an in-house program that assigns the backbone and side-chain conformations that are observed most frequently in α-helices of known structures for each of the 20 amino-acid residues. When severe side-chain clashes occurred, conformations were altered manually by selecting alternative conformations that still occur frequently in known structures. Segments that did not correspond well to any of the templates (linkers, selectivity filters, and VSDs of closed conformations) were modeled manually, choosing conformations that satisfied a series of criteria regarding energetically favorable interactions among protein, water, and lipids, exposure of poorly conserved residues, and interactions among highly conserved residues (13). Invacu energy-minimization calculations were then performed using CHARMM (14). The minimization was conducted while constraining the model to fourfold symmetry by generating identical neighboring subunits and placing them symmetrically about the central axis of the pore. Thus, each of the four subunits has a conformation and interactions with neighboring subunits identical to those of the other subunits throughout the minimization process. On a global scale, this process does not alter the structure significantly; it primarily eliminates some bad van der Waals contacts, improves electrostatic interactions of hydrogen bonds and salt bridges, and adjusts some bond lengths and angles, especially in locations where segments were connected manually. Yet, because of the nature of the minimization process, some small possible errors may be introduced into the model. Hence, the minimized structures were examined manually, to detect any distortions of secondary structure or inconsistencies with other modeling criteria. Structures were then adjusted manually to eliminate or reduce these potential errors. The iterative process of manual adjustment and symmetric minimization was repeated until no noticeable improvement (i.e., satisfaction of modeling criteria) was observed. This process usually requires ~4 iterations.

Preliminary models were then centered with and embedded in a pre-equilibrated phosphatidylethanolamine (POPE) lipid bilayer, with water on each side and ions in the pore. A characteristic system included, with the protein, ~350 lipid molecules and ~30,000 water molecules. The typical dimensions of the system were $14 \times 14 \times 10$ nm^3.

The first step involved minimizing the protein structure in the presence of lipids and water until energetic minima criteria were achieved. Then the system was equilibrated for 500 ps, during which time the structure of the protein remained fixed, and lipids and water molecules were allowed to equilibrate. The final step was to perform all-atom MD.

In initial MD simulations, the structure of the PD was constrained during the first nanosecond of the first simulation, to allow the VSD to move without distorting the PD. The addition of lipid, water, and ions makes the models more complete, and the simulations should allow the structures to escape some local energy wells. A time-averaged structure during the last 0.5 ns of the simulation was calculated and compared with the original model at the beginning of the simulation. In those portions of the models where systematic changes occurred in most or all of the subunits (e.g., if most of the L4–5 segments shifted in the same direction relative to the pore, or if side-chain conformations of specific residues changed in the same way in most subunits), new symmetric models were generated from the subunits or different portions of subunits that were visually judged to best reflect the average conformation and location of each segment during the last nanosecond of the simulation, and that best maintained the secondary structure of the original models. The revised model was energetically minimized again with fourfold symmetry constraints, and another MD simulation was performed. This it-

erative process was repeated for both open and closed structures until systematic adjustments in the subunit structures were no longer observed. In total, 36 simulations, most of which were 6 ns long, were performed in the course of this project. A final 10-ns MD simulation was performed, to better evaluate the stability of each major model.

The MD simulations were run using the program Gromacs (15). Coordinates for the POPE lipid bilayer were kindly provided by Dr. Peter Tieleman. Electrostatic calculations were performed using the particle-mesh Ewald method, and the Van der Waals cutoff was 1.0 nm. The time step was 2 fs, and the LINCS algorithm was used to constrain bond lengths. The simulations were run under conditions where the number of atoms, the pressure, and the temperature were kept constant. The protein, lipid, and water were each coupled separately to a temperature bath at 310 K, with a coupling constant τT of 0.1 ps, and at a constant pressure of 1 bar in all directions, with a pressure constant of $\tau p = 1.0$ ps. Sodium ions were placed at the putative binding sites in the selectivity filter and the cavity. Each simulation was preceded by an energy minimization, using the steepest-descent method. This was followed by a short equilibration run of 500 ps, with harmonic constraints on the backbone atoms of the protein to allow packing of the lipid molecules around the protein and relaxing of the water molecules. Initial simulations were run for 6 ns, using the Biowulf parallel computing cluster of the National Institutes of Health (www.biowulf.nih.gov), which took ~2 days or less, depending on the number of CPUs used. After the consensus, candidate stable structures were obtained, longer simulations were performed (10 ns for the final simulation) to ensure stability. The nonbonded interaction-energy calculations were based on the contributions of the Coulombic short-range, Lennard-Jones short-range, and long-range potential interaction energies, averaged over the last half of the simulation periods.

Molecular graphics images were produced using the Chimera package (16) from the Resource for Biocomputing, Visualization, and Informatics at the University of California, San Francisco (supported by National Institutes of Health grant P41 RR-01081).

After models were developed as described above, two new K^+-channel crystal structures were ascertained. The PD of the crystal structure of a chimera of Kv1.2 and Kv2.1 channels (2) was very similar to that of the Kv1.2 crystal structure that we used as a template for the open conformation, and thus led to no substantial changes in our models of the open PD. However, its higher resolution influenced the models of the VSD described in our accompanying study. The crystal structure of the MlotiK channel (4) is the first 6TM channel to be crystallized in a closed conformation. This may be significant, because it provides a template for modeling the S4–S5 linker (L4–5), and its S5 helix is more likely to be a better template for 6TM channels than is the analogous segment of the 2TM KcsA channel. We thus remodeled the closed conformation using the MlotiK crystal structure, and performed iterative MD simulations as described above. We report here on the final model based on these simulations.

RESULTS

Sequence alignments and conservation

The first crucial step in developing a homology model is to align the sequence of the target protein with that of the template. For distantly related proteins, such as NaChBac and K_v channels, the correct alignment is often difficult to discern. However, if the protein belongs to a large family, much of the ambiguity can be reduced by aligning many homologous sequences. The helical net representations of the transmembrane segments of NaChBac and K_v in Fig. 2 are colored according to a mutability score (13) that we calculated from multisequence alignments of 243 NaChBac homologues (67 from prokaryotic genomes, and 176 from marine samples) and 273 K_v homologues (see also the linear alignment of sequences in our accompanying study). Alignment of the VSD is discussed in our accompanying study. Sequences of the PD are difficult to align. Although these segments have numerous positions that are highly

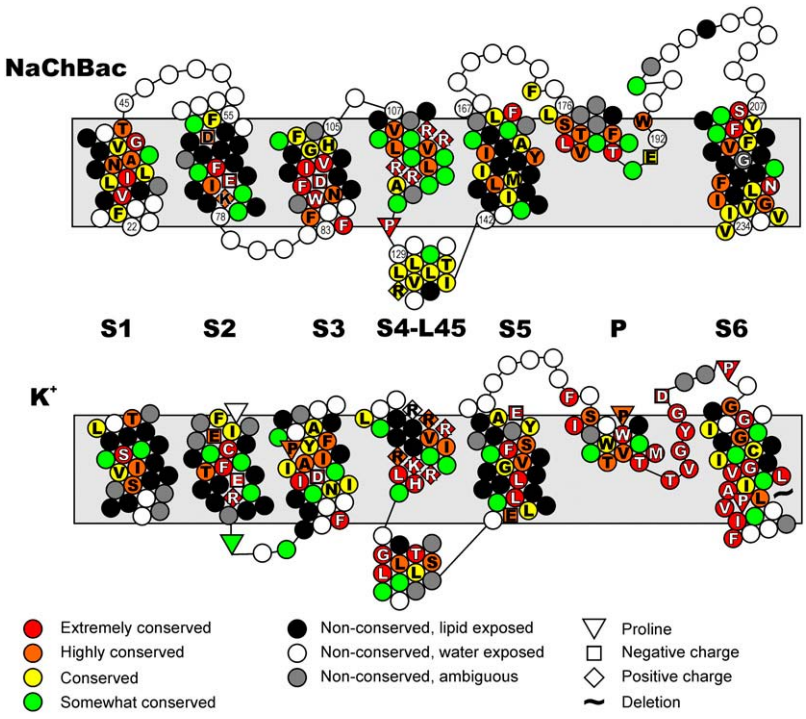

FIGURE 2 Helical net representation of NaChBac (*top*) and K_v (*bottom*) channel protein sequences. Positions are colored according to mutability (13) within a family, as indicated at bottom. Solid circles represent nonconserved residues, likely exposed to lipids (mainly hydrophobic). Open circles represent nonconserved residues, likely exposed to water (mainly hydrophilic). Gray circles represent nonconserved residues, likely exposed to lipid headgroups (hydrophobic and nonacidic hydrophilic). Special residue types are denoted by diamonds for basic residues (*R* and *K*), squares for acidic residues (*D* and *E*), and triangles for prolines. A number inside a residue corresponds to the actual position of the residue in the NaChBac sequence. The shaded region represents the lipid membrane. Note the deletion in S6 of the potassium channel. This deletion ensures maximal alignment between conserved residues in S6 of both families, and may cause differences in gating mechanisms between the two families.

conserved *within* each family, few positions are conserved *between* families. We favor the alignment in Fig. 2 for the S4–S5 linker (L4–5), S5, and P segments for the following reasons: 1), there are no insertions or deletions (indels) from the beginning of S4 through the P helix for NaChBac and Kv1.2, and no indels from the beginning of S1 through the P helix for the alignment of NaChBac with MlotiK (see Fig. 2 of our accompanying study); 2), the hydrophobic face of L4–5 is highly conserved both within and between families in this alignment, whereas the hydrophilic face is poorly conserved; 3), in NaChBac, an extremely conserved proline, P127, is positioned as the first residue of the L4–5 helix, a secondary structure position frequently occupied by proline; 4), another NaChBac proline, P142, is positioned at the N-terminus of S5; 5), highly mutable and hydrophobic (Fig. 2, *black*) residues of the N-terminus half of S5 align in the NaChBac and K_v families, and are exposed to lipids in models developed using this alignment; 6), the alignment of the P segment is the one often identified as best by multisequence alignment algorithms such as ClustalW (17), and a phenylalanine preceding the P segment and a threonine at the end of the P-helix are conserved both within and between the two families (F174 and T189 of NaChBac); and 7), NaChBac, Ca_v and Na_v P segments often contain sequences consistent with amphipathic α-helices. The selected alignment orients the polar face of the putative NaChBac helix formed by T183 and Q186 (analogous residues in Ca_v and Na_v are also usually hydrophilic) toward the pore. Alignment of the second part of the P segment that actually forms the selectivity filter in K^+ channels is even more difficult and almost pointless, because the backbone structure of the segment is likely to differ in the two proteins. For example, the backbone carbonyl oxygens form the K^+ binding sites of K^+-channel selectivity filters. However, mutagenesis experiments suggest that side chains form the selectivity filters of Ca_v and Na_v channels (18).

The alignment of the C-terminus portion of S6 is relatively unambiguous for NaChBac and K_v sequences, e.g., four of five residues from NaChBac positions 230–234 (VIVNN) are identical to residues 408–412 (VIVSN) of Kv1.2. The consistency of this alignment with results of scanning cysteine accessibility method (SCAM) studies of S6 segments of open Ca_v channels is discussed below. When the open conformation of S6 is modeled after the Kv1.2 crystal structure using this alignment, most of its hydrophilic residues are exposed, and most of its hydrophobic residues are buried (see Fig. 6). Alignment of the first half of S6 is more difficult. The illustrated alignment was selected because it places poorly conserved hydrophobic residues (Fig. 2, *black*) at NaChBac positions 210, 214, 217, and 220 on the back side of S6 in the models where they interact with lipids, because it aligns very highly conserved residues at NaChBac positions 208 and 212 with very highly conserved residues in Kv1.2, and because it aligns G219 of NaChBac with a highly conserved ''hinge'' glycine of Kv1.2, where S6 is proposed to bend during activation gating (however, this position is poorly conserved among NaChBac homologues). These alignments of different regions of S6 require an insertion in NaChBac relative to Kv1.2 between the two regions. The position where this likely occurs corresponds to the region that is thought to bend during activation gating.

Using the KcsA and MlotiK crystal structures as templates for modeling the closed conformations presents an interesting dilemma. The S6 of MlotiK and the analogous segment of KcsA have relatively undistorted α-helical secondary structures. Structural alignments of homologous proteins of known structure often differ from the apparent best-sequence alignment when the latter predicts an indel within a regular secondary structure element, because indels are rare within such segments and typically occur in loop segments. We faced three choices in developing homology models: 1), use the alignment with an indel in the middle of S6 as we did in modeling the open conformation; 2), use an alignment that eliminates the indel by shifting the N-terminus portion of NaChBac one position to the right; or 3), use an alignment that eliminates the indel by shifting the C-terminus portion one position to the left. After considering the alternatives, we favor the latter (see Fig. 2 in our accompanying study for the alignment of NaChBac with MlotiK for closed models). This alignment maintains a structure similar to that of the open model for the outer portion of the PD. It also orients toward the pore residues analogous to those in Ca_V channels, for which mutations alter the binding of phenylalkylamines (see Discussion). Models of the inner pore developed in this manner also have good qualities, i.e., the core of the S6 bundle is composed of well-conserved hydrophobic side chains (F224, I228, I231, and V235) that should impede ion permeation. In addition, phenyl rings of F221, F224, and F227 of adjacent subunits interact in a manner likely to be energetically favorable. Moreover, poorly conserved hydrophilic side chains of the C-terminus portion of S6 (N233, N234, E236, and K237) are on the exterior of the bundle, where they can be hydrated. Finally, poorly conserved hydrophobic residues of the N-terminus portion of S6 are exposed to lipids in both open and closed models. This structure is likely to be more stable than one distorted in the middle by an insertion.

Consequences for the gating mechanism of using different alignments of S6 in developing homology models for open and closed conformations are discussed below. The general issue regarding the appropriateness of using different alignments in developing homology models of different conformations arises again in the modeling of S4, as discussed in our accompanying study.

Models of the closed pore domain

The development of an initial homology model of the closed NaChBac PD from the KcsA and MlotiK crystal structures was relatively straightforward for the S5, P, and S6 helical segments, where no indels occur. The modeling was compli-

cated by the presence of many aromatic side chains (18 per subunit), because assigning incorrect conformations to such bulky and rigid side chains can deleteriously influence backbone conformations. Initial side-chain conformations were selected to reduce steric clashes. However, final conformations were based on results of multiple molecular dynamic simulations. Extensive interactions among aromatic side chains appear to be an important component of these pores. All but one of the aromatic side chains of each PD subunit interact with other aromatic side chains in our models, and most interact with multiple aromatic side chains (Fig. 3). Such interactions among aromatic side chains should be energetically favorable (19). The presence of this large number of bulky side chains explains why the S5 and S6 segments tended to move radially outward relative to the templates during MD simulations (Fig. 1). The central-cavity portion of the pore just below the selectivity filter is smaller in the closed NaChBac model than in the KcsA template structures, because the F224 side chain extends into the cavity, even though the backbone of the S6 of NaChBac is farther from the axis of the pore (Fig. 3 *D*). The MlotiK crystal structure also has a phenylalanine from each subunit extending into this cavity, albeit from a different position on S6.

The ascending portion of the P segment immediately after the descending P-helix is important because it forms the selectivity filter. Initial models of this portion of the selectivity filter and its linker segments were developed manually, to optimize energetically favorable interactions and interactions among highly conserved residues. For example., hydrophobic residues were buried and, if conserved, were placed to interact with other conserved residues, poorly conserved hydrophilic residues were exposed to water, and the structures were manipulated to optimize formations of hydrophobic-hydrophobic contacts (especially aromatic-aromatic contacts), hydrogen bonds, and salt bridges. In the initial models, residues 192–198 were assigned a helical conformation, because this segment has characteristics of an amphipathic helix, i.e., when assigned a helical conformation, residues S192 and S195 (where analogous positions are usually hydrophilic and sometimes negatively charged in NaChBac, Ca_v, and Na_v homologues) can form a hydrophilic face, whereas residues W193, V197, and M198 (where analogous positions are usually hydrophobic in NaChBac, Ca_v, and Na_v homologues) form a hydrophobic face. The dipole of this putative helix should be stabilized by the negatively charged E191 residue at its N-terminus and the positively charged R199 residue at its C-terminus. This putative ascending helix was positioned between descending P-helices, with the hydrophilic residues oriented toward the pore. The signature W193 side chain was positioned to interact with signature F185 and T189 side chains and with conserved side chains in S6 (F212 and V216). The two putative P segment helices were then linked in the following way: T189, which is absolutely conserved among NaChBac

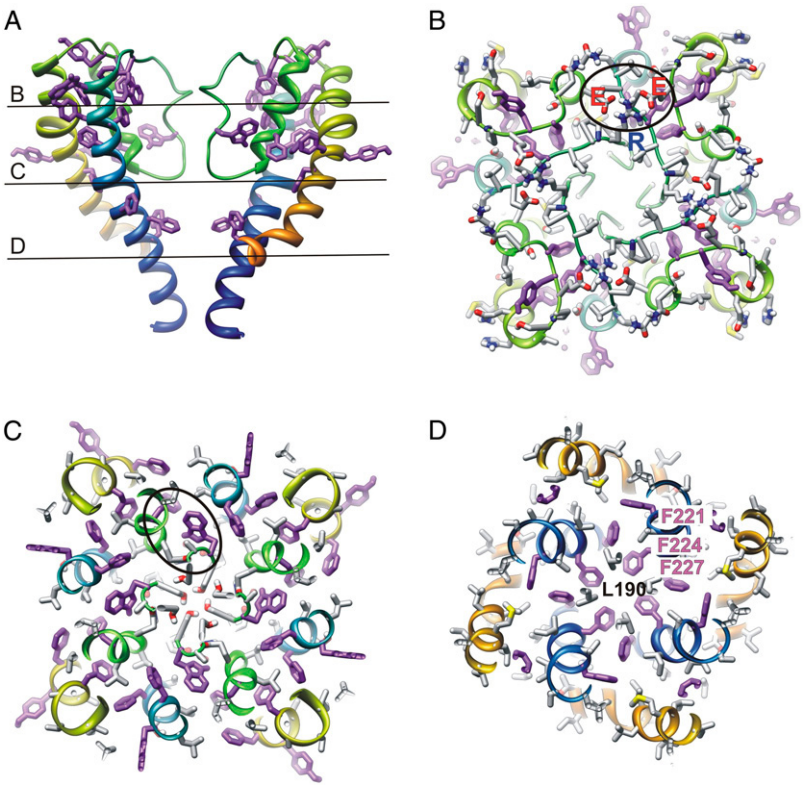

FIGURE 3 Closed model PD shows side chains, with backbone given rainbow colors from orange to blue. (*A*) Side view of two diagonal subunits, with all aromatic side chains colored purple. The lines approximate boundaries between cross sections shown in parts *B–D*. (*B–D*) Cross sections show all side chains, as colored by element or type (*red*, oxygen; *blue*, nitrogen; *white*, hydrogen; *gray*, carbon; and *purple*, aromatic). A set of salt-bridging interactions between E172, E204, and R199 is circled in *B*. A cluster of signature residues is circled in *C*. Interactions among L190, F221, F224, and F227 in the central-cavity region is shown in *D*.

homologues and aligns with the conserved T373 of Kv1.2, was made the C-cap residue of the descending helix. In the initial models, the signature E191 side chain was positioned to form part of the pore lining, where it is relatively exposed to water, but this position changed during MD simulations, as explained below. This arrangement requires the putative ascending P-helix to be on the clockwise side of the descending helix when viewed from the outside. Next, the ascending P-helix was connected to the S6 helix. Assuming the same intersubunit location of S6 relative to S5 as in Kv1.2, the end of the ascending helix is relatively far from the beginning of S6. This requires the linker to have a relatively extended conformation, and may explain why this portion of NaChBac is five residues longer than the analogous region in the K^+-channel templates. The P–S6 linker was modeled to interact favorably with the S5–P linker, i.e., antiparallel β backbone hydrogen bonds form between extended portions of the two linkers, and the highly conserved F202 side chain is buried in an aromatic cluster where it interacts with aromatic side chains of S5 (F158), the S5-P linker (Y173 and F174), and S6 (W209 and F212) residues. The side chains of E172 of the S5-P linker and E204 of the P-S6 linker were positioned to be exposed and salt-bridged to R199, located at the end of the ascending helix. This neutralization of the positive charge of R199 may be important for lowering the electrostatic barrier to the entry of cations into the selectivity filter.

The iterative process of symmetric minimization and asymmetric MD simulations altered the preliminary models in potentially important ways. In the selectivity filter, the carboxyl group of the signature E191 side chain moved away from the pore and formed hydrogen bonds with the side chains of the signature T189 and W193 side chains (Fig. 4 *A*). This clustering of the signature residues away from the lining of the pore is interesting, and suggests that these interactions are crucial to maintaining the structure of the selectivity filter. The S192 and S195 side chains and backbone of G196 formed the narrowest openings through the selectivity filter. This result is consistent with the finding that S192D and S195D mutations dramatically increase P_{Ca}/P_{Na} (9), the ratio of the permeability of Ca^{2+} relative to Na^+. The helical conformations of S195, G196, and M198 were not maintained in some simulations, and parallel β-type backbone hydrogen bonds formed between M198 and F202 of adjacent subunits. Although these changes did not greatly alter the position of the residues, they weakened the hypothesis that the ascending part of the selectivity filter has a regular helical conformation; i.e., it may have a coiled or distorted helical conformation. In these simulations of the closed conformation, the L190 side chain moved to a position relatively near the axis of the pore, where its hydrophobic side chain interacted with hydrophobic side chains of S6 residues I223, F224, and F227 (Fig. 3 *D*). The simulations also caused the L4–5, S5, and S6 segments to move radially away from the pore, increased the tilt of S5, and caused L4–5 to move farther into the transmembrane region.

Models of the open-pore domain

Modeling of the open-pore domain was more complicated for the following reasons: 1), the VSD appears to have a greater effect on the conformation; 2), the positions of S6 in crystal structures of open K^+ channels differ substantially, and the core of the pore domain is less densely packed; 3), in our models, an insertion occurs near the middle of S6 in NaChBac relative to the Kv1.2 template; and 4), the open-pore models were less stable during MD simulations. Thus, the open-pore models are more ambiguous.

Although the selectivity filter may remain relatively unaltered from that of the closed model, it is also possible that its conformation changes. The conformation of T189, L190, and E191, located at the end of the P helix, is especially ambiguous. In the closed conformation described above, the L190 side chain is relatively near the axis of the pore, whereas E191 extends away from the pore. This portion can also be modeled for both closed and open channels, so that the L190 side chain is oriented away from the pore, whereas the E191 side chain extends into the inner pore region (Fig. 4 *B*). The disadvantage of this second conformation is that few of the signature side chains interact, and the hydrogen bonding within this region is not as complete as in the model of Fig. 4 *A*. However, the advantages for the open conformation are that the hydrophobic L190 side chain has more interactions with other hydrophobic side chains and is located away from the pore where it would present less of a hydrophobic barrier to permeation, and the E191 side chain extends into the inner pore, where it can be more hydrated and should lower the electrostatic barrier to cation permeation. An orientation of the E191 side chain into the pore is also more consistent with the results of SCAM studies of eukaryotic Na_V-channel and Ca_V-channel P segments (see Discussion). We performed multiple MD 6-ns simulations, using both P segment conformations in both open and closed models. As might be expected, the closed conformation was slightly more stable, especially for the E191 side chain. However, we never observed a transition from one conformation to the other. This suggests that the barrier between these configurations is relatively high. Although we favor the first configuration for the closed state, the alternative ''open'' configuration is presented here, because we cannot exclude the possibility that this type of transition occurs during gating.

The way that S6 bends during activation may be another importance difference between NaChBac and K_v channels. The insertion near the middle of S6 was made initially by manually connecting portions of the homology models that preceded and followed N225. However, N225 and immediately preceding residues adopted a helical conformation during MD simulations. The ''bulge'' propagated up the S6 helix, primarily to the T220 residue, leaving the S6 helix of the final model distorted from G219 through I222. The G219 corresponds to the putative ''glycine hinge'' advocated for K^+ channels. Mutation of G219 to proline stabilizes the open

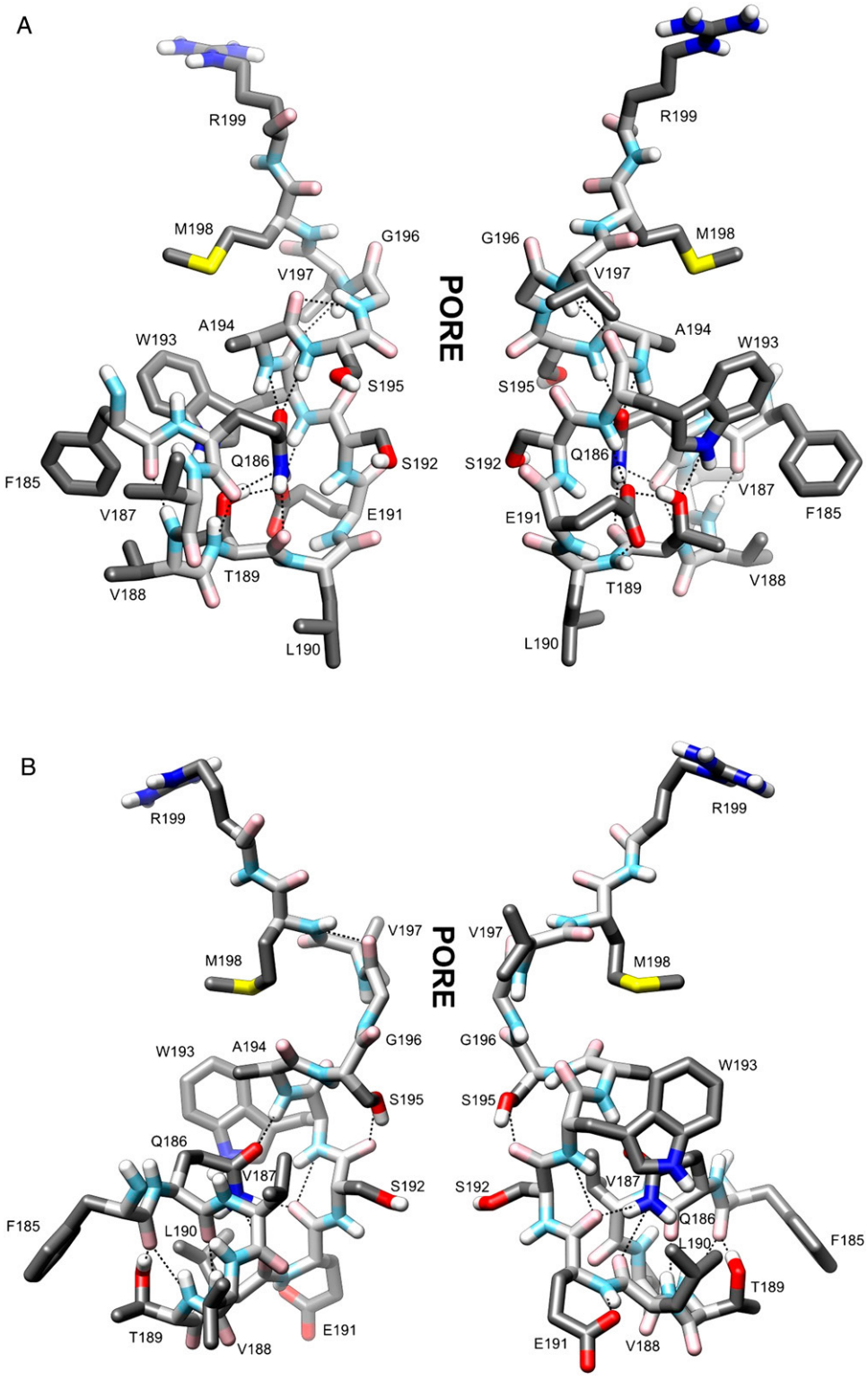

FIGURE 4 Stick representation of selectivity filter residues 185–199, with side view of only two diagonal subunits. Atoms are colored by element, with backbone in lighter shades. Dashed lines represent hydrogen bonds. (*A*) Closed model. Signature residues (F185, T189, E191, and W193) interact to form a dense, stable network of hydrogen bonds and aromatic-aromatic interactions best seen in the right subunit. (*B*) Possible model for an open pore. The primary differences from the closed model are that the E191 side chain has moved into the inner pore where it may be hydrated, and the L190 side chain has moved farther from the pore, where it may interact with hydrophobic residues of S6 segments.

conformation and slows inactivation, indicating that this region is important for activation gating, and suggesting that S6 is distorted in this region when the channels is open (11). This distortion is stabilized by hydrogen bonds formed from the side chain of N225 to the backbone oxygens of T220 and F221 (Fig. 5). These interactions may explain why N225 is the most highly conserved S6 residue both within and between NaChBac, Ca_v, Na_v, and TRP channels. The C-terminus portion of S6 below the kink forms an amphipathic α-helix in which N225, G229, N233, N234, E236, and K237

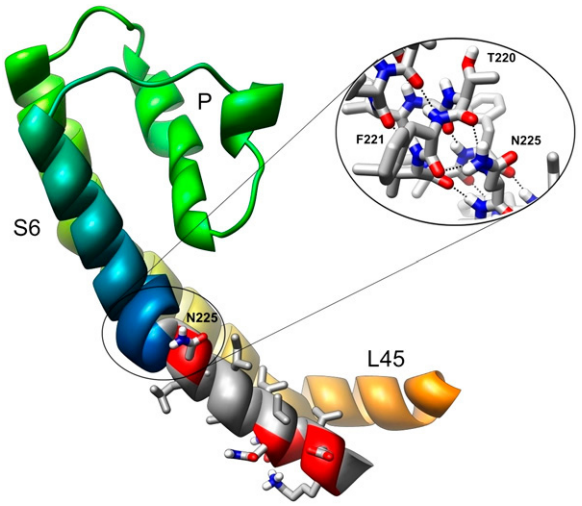

FIGURE 5 Side view of one subunit of $Open_1$ conformation PD. Most subunit are colored as in Fig. 1 and only the backbone is shown, but the C-terminus half of S6 is in gray for apolar residues, and red for polar residues, and side chains are colored by atom. A kink in the S6 helix is stabilized by hydrogen bonds between the N225 side chain and the backbone oxygen atoms of T220 and F221 (for details, see *inset*). S6 is amphipathic below this distortion. The hydrophobic face (*gray*) interacts with hydrophobic residues on L45, S5, and the S6 from adjacent subunit (not shown), whereas polar residues (*red*) are exposed to water in the pore and cytoplasm.

form the more polar face. These are oriented toward the pore or cytoplasm in the model, whereas the more hydrophobic residues tend to be more buried, i.e., they interact with hydrophobic residues of L4–5, S5, and adjacent S6 segments (Fig. 6).

The positions of L4–5, S5, and S6 appear to depend on the conformation of the VSD. When the alignment in Fig. 2 (or alignment 1 in Fig. 2 of our accompanying study) was used for S4 of the VSD, the positions of these segments remained fairly near analogous residues of the Kv1.2 or Kv1.2/2.1 chimera (for later simulations) templates. However, these models appear to be inconsistent with the magnitude of the NaChBac gating charge (see accompanying study). Shifting the alignment of S4 by three positions to the left for NaChBac eliminates this problem. However, simulations of models with the shifted S4 caused the inner-pore region formed by L4–5, S5, and S6 to expand radially (compare Fig. 6, *B* and *C*). These expanded structures are more consistent with LRET studies (20) of residues in depolarized NaChBac channels (see accompanying study). Our working hypothesis is that the initial or $Open_1$ model in Fig. 6 *B* may be reasonable for a transition conformation, but that the open conformation is likely to have a more expanded inner pore, similar to the $Open_2$ model in Fig. 6 *C*. However, it is also feasible that the $Open_1$ model corresponds better to an open conformation, and that the $Open_2$ model actually corresponds better to an inactivated conformation.

These models are also consistent with the results of SCAM studies performed on S6 of the Cav2.1 channel (21). Analogous residues at positions that, when mutated to cysteine, are accessible to [2-(trimethylammonium)ethyl]-methanethiosulfonate (MTSET) in all four homologous repeats and all reside on the face of the helix that is oriented toward the pore (Fig. 6 *D*, *red*). Positions analogous to N225 were included as well. These positions were accessible when mutations were introduced in two repeats, whereas the protein failed to express when the mutations were introduced in the other two repeats. All positions that were inaccessible to MTSET in all four subunits faced away from the pore (Fig. 6 *D*, *blue*). A few positions on the more outwardly oriented faces of the S6 helices were also accessible to MTSET in some, but not all, homologous repeats. These few potentially inconsistent results could be attributable to distortions in the structures introduced by the mutations, or to differences among the four homologous repeats.

Models of L226P mutants

Mutating L226 to proline has the unusual effect of reversing the polarity of voltage-dependent gating, i.e., the L226P channel opens at negative voltages, and closes at positive voltages (10). Proline occurs frequently at the first position of an α-helix, but tends to inhibit helical conformations for the preceding residue (22). For NaChBac, the preceding residue is N225. Asparagine residues often serve as N-cap residues (22) (i.e., the last nonhelical residues preceding an α-helix), and they often have the backbone torsion angles of a left-handed helix (23). Thus we have explored whether, in the L226P mutant, the normally helical N225 residue switches to a left-hand conformation, causing the helix to break and rotate $\sim$200° relative to the pore. Fig. 7 illustrates the consequences of this type of conformational change for our models of both closed and $Open_1$ conformations. For the closed conformation, the break and rotation of the helix disrupt the hydrophobic interactions near the axis of the pore by causing the C-terminus portions of S6 helices to move away from the pore and pack in the ''corners'' of a square formed by the four L4–5 segments. The hydrophobic face of this portion of S6 helices is then oriented away from the pore, and interacts with hydrophobic residues of S5 and L4–5, whereas the more polar face of S6 forms the lining of a pore through which ions may flow (Fig. 7 *D*). This type of conformational change has the opposite effect for the wild-type open conformation. The rotation about N225 disrupts the hydrophobic packing of the C-terminus portion of S6 with L4–5, S5, and other S6 segments, and allows hydrophobic faces to self-associate at the axis of the pore, thus occluding it (Fig. 7 *C*).

Final MD simulations

Once relatively final models were developed, as described above, they were submitted to longer MD simulations of 10 ns to analyze their stabilities better. The results of these simulations for closed and open conformations are illustrated three ways in Supplementary Fig. S1 and Fig. S2, and in Fig. 8. The root mean-square deviation (RMSD) versus time plots show the magnitude of the deviation of all atoms of the

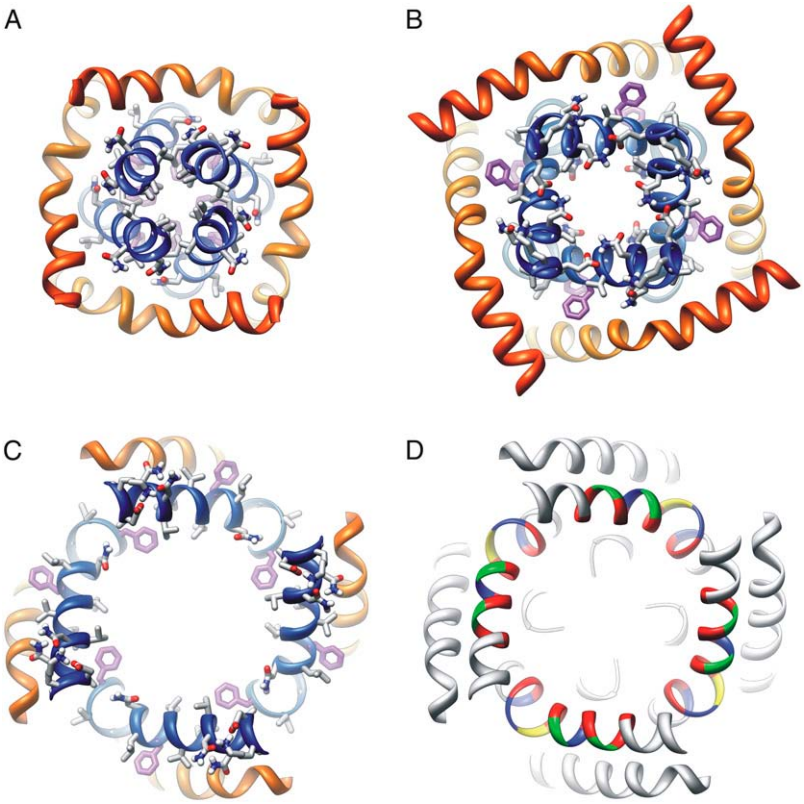

FIGURE 6 View from inside the PD of S6 (*blue*), surrounded by L4–5 and S5 segments (*orange*). Segments and S6 side chains are colored as in Fig. 3. In the closed conformation (*A*), the pore is lined with hydrophobic residues F224 (*purple*), I231, and V235, and polar asparagine side chains (N225, N233, and N234) are oriented away from the pore. In the $Open_1$ (*B*) and $Open_2$ (*C*) models, the hydrophilic S6 side chains of N225, N233, N234, E236, and K237 are exposed to water in the cytoplasm or pore, whereas most of the hydrophobic side chains interact with other hydrophobic residues of adjacent segments. (*D*) SCAM results from S6 segments of a homologous $Ca_v2.1$ channel superimposed on the NaChBac $Open_2$ model. Red indicates that analogous residues in $Ca_v2.1$ were accessible to MTSET in all four repeats. Green and yellow indicate accessibility to MTSET in some (but not all) repeats. Blue indicates no accessibility in any repeat. White residues in S5 and S6 were not mutated.

structure from the symmetric model at the beginning of the simulation. The final simulation of the closed and $Open_2$ conformations were quite stable for the pore domain, whereas the RMSD from the original models stabilized at ~0.3 nm for the last 3 ns of the 10-ns simulation (Supplementary Fig. S1). By comparison, the pore domains of the recently determined Kv1.2/Kv2.1 chimera and MlotiK structures stabilized at ~0.18 nm and 0.38 nm RMSD. The RMSD values for the $Open_1$ and $Open_2$ conformations were ~0.5 nm greater, but remained relatively constant throughout most of the simulations. The greater deviation of the open conformation may reflect the less dense packing of the inner portion of the open pore.

The root mean-square-fluctuations (RMSF) versus position graphs (Supplementary Fig. S2) illustrate how much each residue fluctuated relative to its average conformation during the last nanosecond of the simulation. These RMSF values are indicative of the mobility of specific residues, similar to the B values of crystal structures. As expected, the fluctuations are smaller for helical residues (indicated by a white background). The RMSF for the putative ascending helix of the P segment in both open and closed conformations is as low as for any other segment. The stability of the P segment is noteworthy because the selectivity filter it forms is one of the most important parts of the model, but is also one of the most tentative parts, because the ascending segment was not modeled from a template. The dynamic nature of the first part of S1 and the last part of S6 is probably an artifact attributable to an absence in the models of the segments that precede and follow S1 and S6.

Changes in the NaChBac backbone structure during the simulations are illustrated in Fig. 8, in which the average backbone structure during the last nanosecond of the simulation is superimposed on the symmetric static model at the beginning of the simulation. The symmetric model is intended to represent the type of time-averaged model that would be observed in a crystal structure, whereas the simulated model is more indicative of how the protein could deviate from that structure at any instant. This comparison indicates that the helical segments remain intact and do not move much during the simulation, and that the connecting loops and N-termini and C-termini ends of the model are more mobile.

DISCUSSION

The models and sequence analyses presented here suggest that NaChBac channels have both important similarities to, and differences from, K_v channels. The greatest similarities occur in the VSD and L4–5 linker, suggesting that these two families of channels have similar voltage-sensing mechanisms, and that the movement of the S4 voltage sensor is coupled, via the L4–5 linker, to activation of the S6 gate in similar ways. The greatest differences occur in the P and S6 segments of the PD. These segments of NaChBac are much more like analogous segments in Ca_v and Na_v channels than in K_v channels. Substantial differences in the P segments are to be expected, because the function of these segments, to determine the selectivity of the pore, is obviously different in

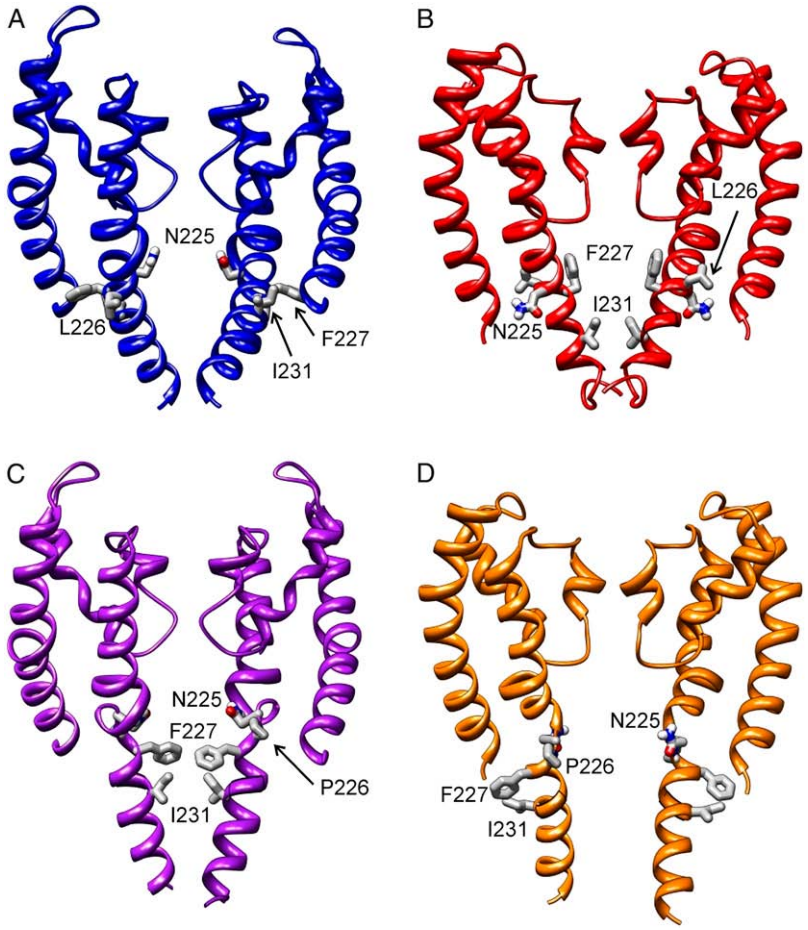

FIGURE 7 Models of how a mutation of L226 to proline may reverse the polarity of channel gating. (*Top*) The channel modeled in its wild-type forms: open (*A*, *blue*) and closed (*B*, *red*). (*Bottom*) Mutated structures. Whereas structure in *C* (*purple*) is in ''open'' conformation, the rotational kink at N225 introduced by the proline causes the hydrophobic residues in the C-terminus of S6 to occlude the pore, hence rendering the channel closed for ion permeation. Likewise, most of the structure depicted in *D* (*orange*) is the original closed structure. However, the additional rotational kink causes hydrophobic residues to point away from the pore, effectively opening the channel for ion permeation.

the different families. The most likely reason that NaChBac does not form a Ca^{2+} channel, despite being more similar to eukarotic Ca_v than to Na_v channels, is the presence of serine instead of a negatively charged residue at positions 192 and 195, which form the narrowest part of the pore, and possibly the presence of an electrostatic barrier created by R199 at the outer entrance to the selectivity filter and a hydrophobic barrier created by L190 at the inner exit from the selectivity filter of the first model. The clustering in our models of the signature residues (F185, T189, E191, and W193) to form a stable structure with multiple hydrogen bonds and aromatic-aromatic interactions may explain why these residues are so well-conserved among NaChBac and Ca_v channels. Energetically favorable interactions among these and surrounding residues may explain why the positions of the residues of the ascending portion of the selectivity filter do not fluctuate much during MD simulations. This segment may need a rather static structure to maintain the selectivity of the pore for Na^+ ions. The reason for the differences in S6 segments is less clear. Maybe it is related to differences in the P segments, because the S6 segments interact with the P segment in the region where the NaChBac model of S6 differs most from that of Kv1.2. In our models, S6 not only bends during activation, but the inner half also rotates more than was proposed for K^+ channels. The absolutely conserved N225 residue appears to be important for stabilizing the open conformation. Understanding the structure and gating mechanism of the NaChBac S6 segment may be valuable for understanding the gating mechanisms of other channels with similar S6 sequences, i.e., Ca_v, Na_v, and even TRP channels.

We imposed fourfold symmetry for our initial models, for models at the beginning of each iterative MD simulation, and for our final models. This assumption is valid for most known channel structures, and has served us well in developing models in the absence of known structures. For example, a model from our laboratory of the signature-sequence part of the selectivity filter of an inwardly rectifying K^+ channel, published in 1995 (18), was virtually identical to that subsequently determined by crystallization (see Supplementary Fig. S3). This degree of accuracy would not have been possible without symmetry constraints. Nonetheless, perfect symmetry of time-averaged structures at equilibrium is not an absolute necessity. We typically observed asymmetry during MD simulations, and in some instances, the closed conformations appeared to adopt an ~2-fold symmetry, in which P and S6 segments of two opposing subunits moved farther from the pore, whereas those of the intervening subunits moved toward the pore. Thus, we are not certain that the

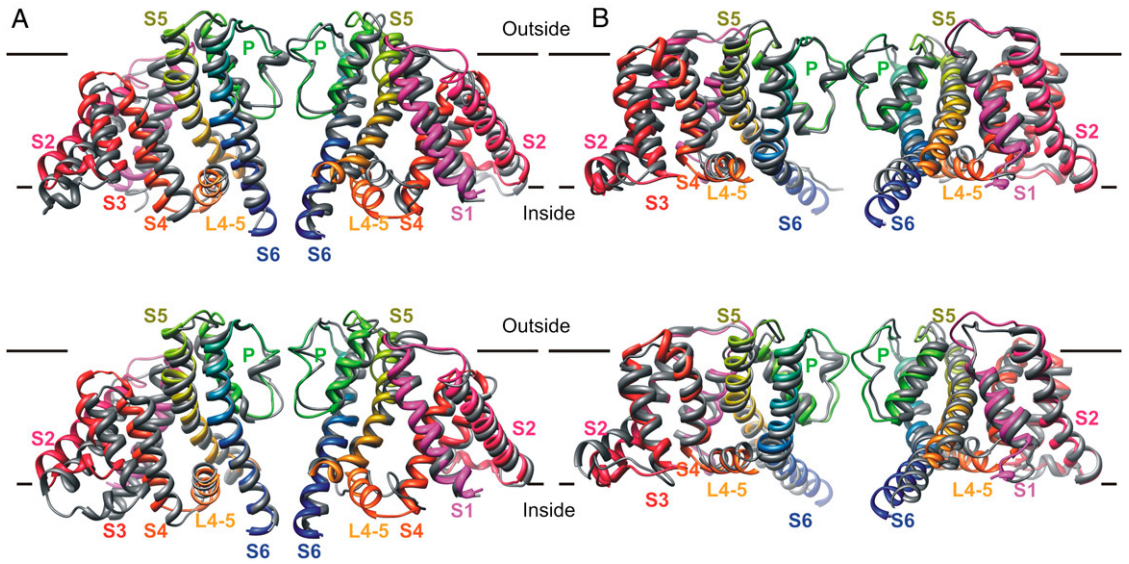

FIGURE 8 Ribbon representations of deviation of backbone structure, averaged over last nanosecond of the simulation (*gray*) from the original symmetric structure (*rainbow-colored*) in the (*A*) $Closed_{0a}$ and (*B*) $Open_2$ models. For an uncluttered view, only domains from two opposite subunits are shown. Structures at bottom are rotated by 90° about the *y* axis relative to the top structures, so that all four subunits can be seen. Segment labels are colored according to color of the segment in symmetric models.

assumption of fourfold symmetry is valid at equilibrium, and asymmetry probably occurs during the gating process.

The dramatic reduction of the rate of inactivation by a G219P mutation within the S6 hinge region (11) is consistent with an inactivation of NaChBac because of conformational changes within the P segment, insofar as G219 interacts with the P segment. We can envision many ways in which permeation through the NaChBac pore might be impeded by changes within the P segment; e.g., during MD simulations, we observed R199 block the outer entrance, L191 block the inner exit from the selectivity filter, and asymmetric collapses of the ascending part of the P segment block the pore. However, the asymmetric structures were never the same in different simulations, and it would be speculative to attribute inactivation to any of these processes.

We view NaChBac as a stepping-stone structure for modeling the structure and functional mechanisms of Ca_v and Na_v channels, and we have collaborated with another group to develop models of the $Ca_V1.2$ channel, based on our NaChBac models (24). For modeling, NaChBac has the advantages of being more similar to K_v channels than are the Ca_v and Na_v channels. Also, they are simpler because they are composed of four identical subunits instead of four homologous repeats, and the loops connecting transmembrane segments are usually shorter in NaChBac. The NaChBac channels have the advantage for experimental structural studies of being prokaryotic, which typically means that it is easier to express more protein for structural studies. The family of prokaryotic channels that includes NaChBac likely contains channels with differing selectivities, i.e., those homologues that have negatively charged residues at positions analogous to S192 or S195, and that do not have a positively charged residue at the position analogous to R199, probably form Ca^{2+} channels. It is difficult to anticipate the selectivity of one subfamily that has serine at the position analogous to the E191 signature residue. Thus, the different types of NaChBac homologues may be interesting for both experimental and theoretical studies of ion-selectivity mechanisms.

Many studies probing the structure and functional mechanisms of eukaryotic Na_V and Ca_V channels have been performed. We used few data from these studies in developing our NaChBac models, because the features of eukaryotic channels may differ substantially from those of NaChBac. Still, it is of interest to determine whether models developed independent of these studies are consistent with them. Results of some of these studies, and their consistencies with our NaChBac models, are discussed below.

Numerous SCAM studies were performed on the P segments of Na_V (25–29) and Ca_V channels (30,31). Most of these studies analyzed the accessibility of residues within the ascending segment to extracellular sulfhydryl reagents. These data are difficult to relate to the NaChBac homotetramer, because the results vary both among the four different homologous repeats and between Ca_V and Na_V channels. Nonetheless, some general patterns have emerged that should be applicable to NaChBac. In general, positions in Na_V and Ca_V channels analogous to the signature E191 and beyond were found to be accessible to most reagents, including MTSET, in most repeats. These findings are more consistent with our models of the open conformation in which the E191 side chain is oriented toward the pore. However, these findings also suggest that the opening through the ascending

segments above the E191 position is larger than in our NaChBac models. This difference may be real, because in NaChBac, the side chains of pore-facing S192, S195, and G196 residues tend to be smaller and less hydrophilic than analogous residues in Ca_V and Na_V channels. The MD simulations of a model of the Cav1.2 channel based on our NaChBac produced a larger opening through the selectivity filter (24). Residues preceding the E191 position were less accessible. In the study by Wu et al. (31) on Ca_V channels, the position analogous to L190 was accessible to MTSET in repeat IV only, but was accessible to the smaller methanethiosulfonate ethylammonium (MTSEA) in all repeats, and the residues analogous to T189 were not accessible to MTSET in any repeat, and were accessible to MTSEA in repeat III only. Likewise, Yamagishi et al. (29) found that in Na_V channels, residues analogous to NaChBac L190 were inaccessible to extracellular Cd^{2+} or MTSEA in repeats I and II, but were accessible to extracellular Cd^{2+} and MTSEA in repeats III and IV, that residues analogous to T189 were inaccessible to MTSEA in all repeats and accessible to Cd^{2+} in repeat III only, and that the residue analogous to V188 was inaccessible to both Cd^{2+} and MTSEA in all repeats. The results for repeats III and IV appear to be inconsistent with our models of NaChBac, but also suggest that in Na_V and Ca_V channels, the conformations of P segments in these repeats differ from those of repeats I and II. Yamagishi et al (29) analyzed the accessibilities of residues of the putative descending P helix of Na_V channels that align with NaChBac residues 177–186. None of the introduced cysteines were found to be accessible to MTS reagents, suggesting that this segment is relatively buried within the transmembrane region, as in our models. The only mutations to cysteine that altered the selectivity of the Na^+ pore were for arginines in repeats I and II that align with Q186. These mutations also reduced the binding affinity of tetrodotoxin (TTX). These results are consistent with our model, because the Q186 side chain is oriented toward the pore, and forms an integral part of the hydrogen-bonding network proposed to stabilize the selectivity filter (Fig. 4). Similar inaccessibilities to MTS reagents were found by Koch et al. (30) in studies of Ca_V for residues analogous to NaChBac 183–188. One study of Na_V channels analyzed accessibilities from both sides of the membrane of the three residue positions (analogous to NaChBac V188, T189, and L190) immediately preceding the signature charges (28). They found no accessibility from the inside to either Cd^{2+} or MTSEA for any of these positions, and no accessibility from the outside to the position analogous to NaChBac residue V188. The inability of these studies to identify residues within P segments that are accessible from the inside is surprising, because other studies suggest that open Na_V and Ca_V channels have a large inner pore through which charged drugs can enter and block the channel near the central region predicted to be just below the P segments. In our models of the open conformation, the VTL residues (positions 188–190) are at the C-terminus of the descending helix, but are all oriented away from the pore and interact with hydrophobic residues of the surrounding S5 and S6 segments. The hydrophobic environment and close packing may prevent reactions of the introduced sulfhydryl group with the reagents.

Numerous studies were also performed to identify residues involved in forming drug-binding sites within the pore of Ca_V and Na_V channels. Positively charged phenylakylamine drugs enter open Ca_V channels from the inside, and become trapped near the midregion of the channel when it closes (32,33). Photoaffinity labeling experiments indicate that these bind to S6 of repeats III and IV. The NaChBac residue positions at which mutations of analogous sites in Ca_V channels were shown to affect drug-binding are 215, 216, 227, and 228 for repeat III, and 216, 220, and 223 for repeat IV. Most of these residues (216, 220, 223, 227, and 228) are on the face of S6, oriented directly toward the pore in our model of the closed conformation (Supplementary Fig. S4 *A*). Other groups (34,35) used the same alignment as ours for the PD of Ca^{2+} channels, based on these data.

Photoaffinity labeling experiments indicate that dihydropyridine (DHP)-type drugs inhibit some Ca_V channels by binding to S6 segments of repeats III and IV, and to the P segment of repeat III. These lipophilic drugs appear to access their binding site from the extracellular side, probably through the lipid phase (33). This site was estimated to be 11–14 Å from the extracellular surface of the membrane. Dihydropyridine appears to inhibit opening of the channel allosterically, by binding to a closed conformation to which one Ca^{2+} ion binds (36). The NaChBac residue positions analogous to those where mutations in repeat III inhibit DHP binding are 151 and 155 of S5; 190, 191, and 198 of P; and 215, 216, 219, and 224 of S6. Those corresponding to sensitive sites in IVS6 are 213, 216, 217, 223, and 224. Our NaChBac models have narrow openings from the lipid phase into the pore located between S5, S6, and S6 of an adjacent subunit just below the end of the descending P helix. Residues 151 and 155 of S5, 190 and 191 of P, 224 of S6 of the same subunit, and 213, 216, and 224 of S6 from the adjacent subunit form part of the lining of this niche (see Supplementary Fig. S4 *B*). We suspect that a similar niche forms the DHP binding site in DHP-sensitive Ca_V channels.

Although the models presented here are unlikely to be precisely correct in every detail, especially for dynamic loop regions, they may be useful in the design and interpretation of experiments. Some types of experiments that could be performed to test these models are suggested in the Supplementary Material (NaChBac-Test-Sup.pdf).

SUPPLEMENTARY MATERIAL

To view all of the supplemental files associated with this article, visit www.biophysj.org

This work was supported by the Intramural Research Program of the Center for Cancer Research, National Cancer Institute, National Institutes of Health.

REFERENCES

1. Jiang, Y., A. Lee, J. Chen, V. Ruta, M. Cadene, B. T. Chait, and R. MacKinnon. 2003. X-ray structure of a voltage-dependent K+ channel. *Nature*. 423:33–41.
2. Long, S. B., X. Tao, E. B. Campbell, and R. MacKinnon. 2007. Atomic structure of a voltage-dependent K^+ channel in a lipid membrane-like environment. *Nature*. 450:376–382.
3. Long, S. B., E. B. Campbell, and R. MacKinnon. 2005. Crystal structure of a mammalian voltage-dependent Shaker family K^+ channel. *Science*. 309:897–903.
4. Clayton, G. M., S. Altieri, L. Heginbotham, V. M. Unger, and J. H. Morais-Cabral. 2008. Structure of the transmembrane regions of a bacterial cyclic nucleotide-regulated channel. *Proc. Natl. Acad. Sci. USA*. 105:1511–1515.
5. Anderson, P. A., and R. M. Greenberg. 2001. Phylogeny of ion channels: clues to structure and function. *Comp. Biochem. Physiol. B Biochem. Mol. Biol*. 129:17–28.
6. Ren, D., B. Navarro, H. Xu, L. Yue, Q. Shi, and D. E. Clapham. 2001. A prokaryotic voltage-gated sodium channel. *Science*. 294:2372–2375.
7. Ishibashi, K., M. Suzuki, and M. Imai. 2000. Molecular cloning of a novel form (two-repeat) protein related to voltage-gated sodium and calcium channels. *Biochem. Biophys. Res. Commun*. 270:370–376.
8. Durell, S. R., and H. R. Guy. 2001. A putative prokaryote voltage-gated Ca(2+) channel with only one 6TM motif per subunit. *Biochem. Biophys. Res. Commun*. 281:741–746.
9. Yue, L., B. Navarro, D. Ren, A. Ramos, and D. E. Clapham. 2002. The cation selectivity filter of the bacterial sodium channel, NaChBac. *J. Gen. Physiol*. 120:845–853.
10. Zhao, Y., T. Scheuer, and W. A. Catterall. 2004. Reversed voltage-dependent gating of a bacterial sodium channel with proline substitutions in the S6 transmembrane segment. *Proc. Natl. Acad. Sci. USA*. 101:17873–17878.
11. Zhao, Y., V. Yarov-Yarovoy, T. Scheuer, and W. A. Catterall. 2004. A gating hinge in Na^+ channels: a molecular switch for electrical signaling. *Neuron*. 41:859–865.
12. Zhou, Y., J. H. Morais-Cabral, A. Kaufman, and R. MacKinnon. 2001. Chemistry of ion coordination and hydration revealed by a K^+ channel-Fab complex at 2.0 Å resolution. *Nature*. 414:43–48.
13. Shrivastava, I. H., S. R. Durell, and H. R. Guy. 2004. A model of voltage gating developed using the KvAP channel crystal structure. *Biophys. J*. 87:2255–2270.
14. Brooks, B. R., R. E. Bruccoleri, B. D. Olafsin, D. J. States, S. Swaminathan, and M. Karplus. 1983. CHARMM: a program for macromolecular energy, minimization, and dynamics calculations. *J. Comput. Chem*. 4:187–217.
15. Van Der, S. D., E. Lindahl, B. Hess, G. Groenhof, A. E. Mark, and H. J. Berendsen. 2005. GROMACS: fast, flexible, and free. *J. Comput. Chem*. 26:1701–1718.
16. Pettersen, E. F., T. D. Goddard, C. C. Huang, G. S. Couch, D. M. Greenblatt, E. C. Meng, and T. E. Ferrin. 2004. UCSF Chimera—a visualization system for exploratory research and analysis. *J. Comput. Chem*. 25:1605–1612.
17. Thompson, J. D., D. G. Higgins, and T. J. Gibson. 1994. CLUSTAL W: improving the sensitivity of progressive multiple sequence alignment through sequence weighting, position-specific gap penalties and weight matrix choice. *Nucleic Acids Res*. 22:4673–4680.
18. Guy, H. R., and S. R. Durell. 1995. Structural models of Na^+, $Ca2^+$, and K^+ channels. *Soc. Gen. Physiol. Ser*. 50:1–16.
19. Burley, S. K., and G. A. Petsko. 1985. Aromatic-aromatic interaction: a mechanism of protein structure stabilization. *Science*. 229:23–28.
20. Richardson, J., R. Blunck, P. Ge, P. R. Selvin, F. Bezanilla, D. M. Papazian, and A. M. Correa. 2006. Distance measurements reveal a common topology of prokaryotic voltage-gated ion channels in the lipid bilayer. *Proc. Natl. Acad. Sci. USA*. 103:15865–15870.
21. Zhen, X. G., C. Xie, A. Fitzmaurice, C. E. Schoonover, E. T. Orenstein, and J. Yang. 2005. Functional architecture of the inner pore of a voltage-gated Ca^{2+} channel. *J. Gen. Physiol*. 126:193–204.
22. Kloczkowski, A., K. L. Ting, R. L. Jernigan, and J. Garnier. 2002. Combining the GOR V algorithm with evolutionary information for protein secondary structure prediction from amino acid sequence. *Proteins*. 49:154–166.
23. Deane, C. M., F. H. Allen, R. Taylor, and T. L. Blundell. 1999. Carbonyl-carbonyl interactions stabilize the partially allowed Ramachandran conformations of asparagine and aspartic acid. *Protein Eng*. 12:1025–1028.
24. Stary, A., Y. Shafrir, S. Hering, P. Wolschann, and H. R. Guy. 2008. Structural models of the Cav1.2 pore. *Channels*. 2:210–215.
25. Chiamvimonvat, N., M. T. Perez-Garcia, R. Ranjan, E. Marban, and G. F. Tomaselli. 1996. Depth asymmetries of the pore-lining segments of the Na^+ channel revealed by cysteine mutagenesis. *Neuron*. 16: 1037–1047.
26. Perez-Garcia, M. T., N. Chiamvimonvat, E. Marban, and G. F. Tomaselli. 1996. Structure of the sodium channel pore revealed by serial cysteine mutagenesis. *Proc. Natl. Acad. Sci. USA*. 93:300–304.
27. Tsushima, R. G., R. A. Li, and P. H. Backx. 1997. Altered ionic selectivity of the sodium channel revealed by cysteine mutations within the pore. *J. Gen. Physiol*. 109:463–475.
28. Yamagishi, T., M. Janecki, E. Marban, and G. F. Tomaselli. 1997. Topology of the P segments in the sodium channel pore revealed by cysteine mutagenesis. *Biophys. J*. 73:195–204.
29. Yamagishi, T., R. A. Li, K. Hsu, E. Marban, and G. F. Tomaselli. 2001. Molecular architecture of the voltage-dependent Na channel: functional evidence for alpha helices in the pore. *J. Gen. Physiol*. 118:171–182.
30. Koch, S. E., I. Bodi, A. Schwartz, and G. Varadi. 2000. Architecture of Ca(2+) channel pore-lining segments revealed by covalent modification of substituted cysteines. *J. Biol. Chem*. 275:34493–34500.
31. Wu, X. S., H. D. Edwards, and W. A. Sather. 2000. Side chain orientation in the selectivity filter of a voltage-gated Ca^{2+} channel. *J. Biol. Chem*. 275:31778–31785.
32. Beyl, S., E. N. Timin, A. Hohaus, A. Stary, M. Kudrnac, R. H. Guy, and S. Hering. 2007. Probing the architecture of an L-type calcium channel with a charged phenylalkylamine: evidence for a widely open pore and drug trapping. *J. Biol. Chem*. 282:3864–3870.
33. Hockerman, G. H., B. Z. Peterson, B. D. Johnson, and W. A. Catterall. 1997. Molecular determinants of drug binding and action on L-type calcium channels. *Annu. Rev. Pharmacol. Toxicol*. 37:361–396.
34. Zhorov, B. S., E. V. Folkman, and V. S. Ananthanarayanan. 2001. Homology model of dihydropyridine receptor: implications for L-type Ca(2+) channel modulation by agonists and antagonists. *Arch. Biochem. Biophys*. 393:22–41.
35. Lipkind, G. M., and H. A. Fozzard. 2003. Molecular modeling of interactions of dihydropyridines and phenylalkylamines with the inner pore of the L-type Ca^{2+} channel. *Mol. Pharmacol*. 63:499–511.
36. Peterson, B. Z., and W. A. Catterall. 2006. Allosteric interactions required for high-affinity binding of dihydropyridine antagonists to Ca(V)1.1 channels are modulated by calcium in the pore. *Mol. Pharmacol*. 70:667–675.